Supplementary Material (ESI) for Dalton Transactions
This journal is © The Royal Society of Chemistry

Immoblization of phosphotungstate through doping in polypyrrole for supercapacitors

Zhihan Chang, Xiaoguang Sang*, Yu Song, Xiaoqi Sun, Xiao-Xia Liu*

Redox reactions of PW_{12}:

$$[PW_{12}O_{40}]^{3-} + e^- \leftrightarrows [PW_{12}O_{40}]^{4-} \qquad \text{R. S1}$$

$$[PW_{12}O_{40}]^{4-} + e^- \leftrightarrows [PW_{12}O_{40}]^{5-} \qquad \text{R. S2}$$

$$[PW_{12}O_{40}]^{5-} + 2e^- + H^+ \leftrightarrows [HPW_{12}O_{40}]^{6-} \qquad \text{R. S3}$$

$$[PW_{12}O_{40}]^{5-} + e^- \leftrightarrows [PW_{12}O_{40}]^{6-} \qquad \text{R. S4}$$

$$[PW_{12}O_{40}]^{6-} + e^- \leftrightarrows [PW_{12}O_{40}]^{7-} \qquad \text{R. S5}$$

Calculations

1. Calculation for single electrode:

The areal (C_a) and specific (C_m) capacitance of a single electrode can be calculated from galvanostatic charge/discharge profile by the following equations:

$$C_a = \frac{I \times \Delta t}{S \times \Delta U} \qquad \text{equ. S1}$$

Where C_a is the areal capacitance (mF cm^{-2}), I (mA cm^{-2}) is the galvanostatic charge/discharge current, Δt (s) is the discharge time, S (cm^2) is the geometrical area of the electrode, ΔU (V) is the charge/discharge potential window.

$$C_m = \frac{I \times \Delta t}{m \times \Delta U} \qquad \text{equ. S2}$$

Where C_m is the specific capacitance (F g^{-1}), m (g) is the mass of active material on the electrode.

2. Charge balance for ASC device:

The charge stored in cathode (Q^+) and anode (Q^-) should be balanced to maximize the performance of the assembled supercapacitor device by the relationship $Q^+ = Q^-$. The charge stored in each electrode depends on the areal capacitance (C_a), the potential window (ΔU) and the geometrical area of each electrode (S) by the following equation:

$$Q = C_a \times \Delta U \times S \qquad \text{equ. S3}$$

Then the following equation can be deduced:

$$C_a^+ \times \Delta U^+ \times S^+ = C_a^- \times \Delta U^- \times S^- \qquad \text{equ. S4}$$

3. Calculations for ASC device:

The volumetric capacitance of an ASC device can also be calculated from galvanostatic charge/discharge profile by the following equation:

$$C_v = \frac{I \times \Delta t}{V \times U} \qquad \text{equ. S5}$$

Where C_v is the volumetric capacitance (F cm^{-3}), I is the galvanostatic charge/discharge current, Δt (s) is the discharge time, V (cm^3) is the volume of the whole ASC device and U is the operating voltage.

The volumetric capacitance of an ASC device can be calculated from cyclic voltammetry profile by the following equation:

$$C_v^{mv} = \frac{\int i(U)dU}{v \times V \times U} \qquad \text{equ. S6}$$

Where C_v^{mv} is the volumetric capacitance (F cm^{-3}), V (cm^3) is the volume of the whole ASC device, v is the scan rate, U is the potential window in the CV curves, and $i(U)$ is the voltammetry current on the profile.

The energy density (E, mWh cm^{-3}) and power density (P, mW cm^{-3}) of an ASC device can be calculated by the following equations:

$$E = \frac{1000}{2\times 3600} C_v U^2 \qquad \text{equ. S7}$$

$$P = \frac{3600\times E}{t} \qquad \text{equ. S8}$$

Where C_v is the volumetric capacitance (F cm^{-3}), U (V) is the operating voltage and Δt (s) is the discharge time.

Figures

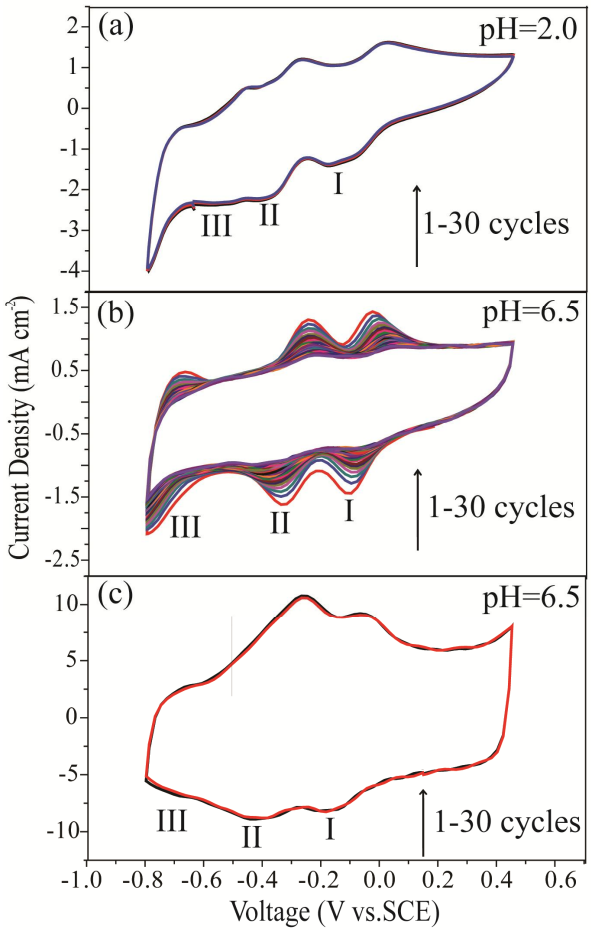

Fig. S1. CV profiles of PW_{12} anions in neutral solution (a) and acidic solution (b), together with that of ECNT-PPy/5PW_{12} in neutral solution (c) at a scan rate of 5 mV s^{-1}.

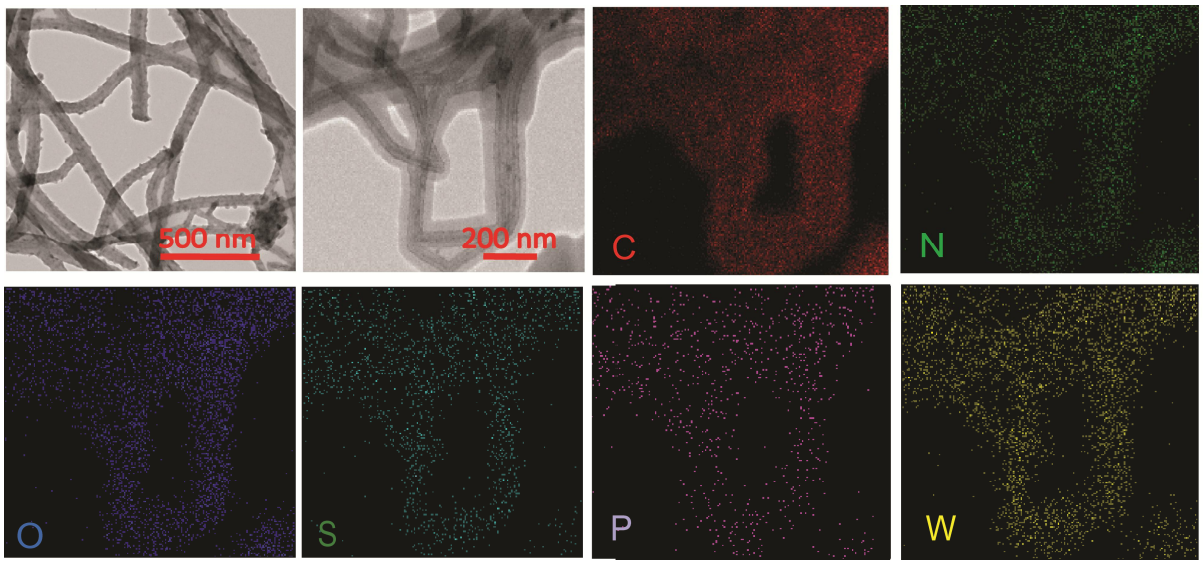

Fig. S2. TEM and elemental mapping images of ECNT-PPy/5PW_{12}.

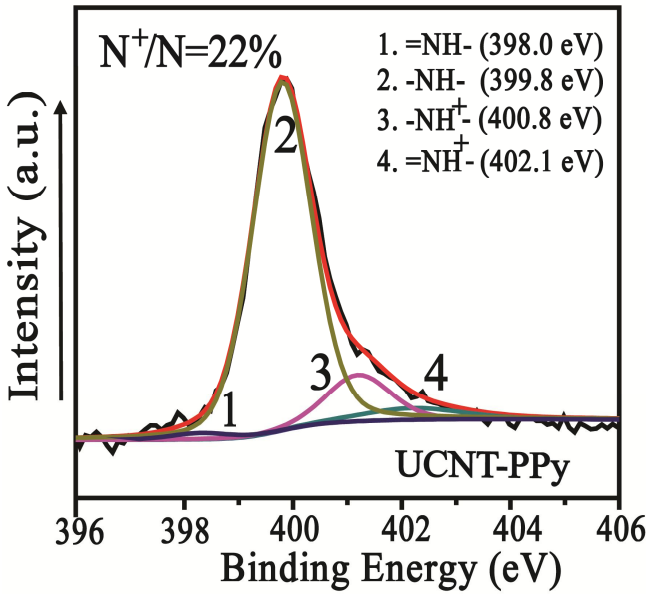

Fig. S3. N 1s XPS core level spectra of UCNT-PPy.

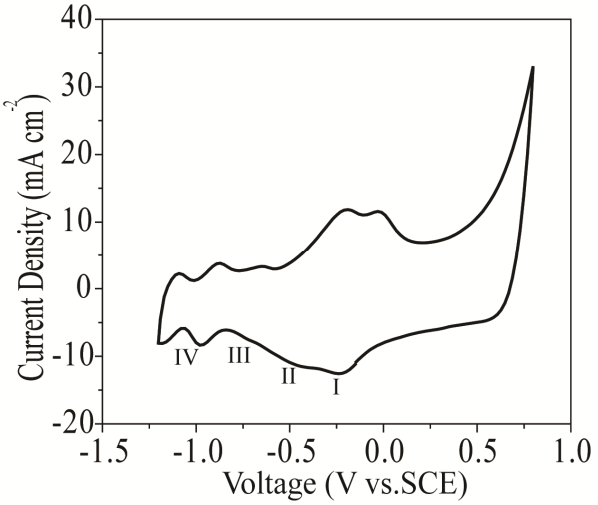

Fig. S4. CV profiles of ECNT-PPy/5PW_{12} in the potential window of -1.2 to 0.8 V *vs*. SCE at a scan rate of 5 mV s^{-1}.

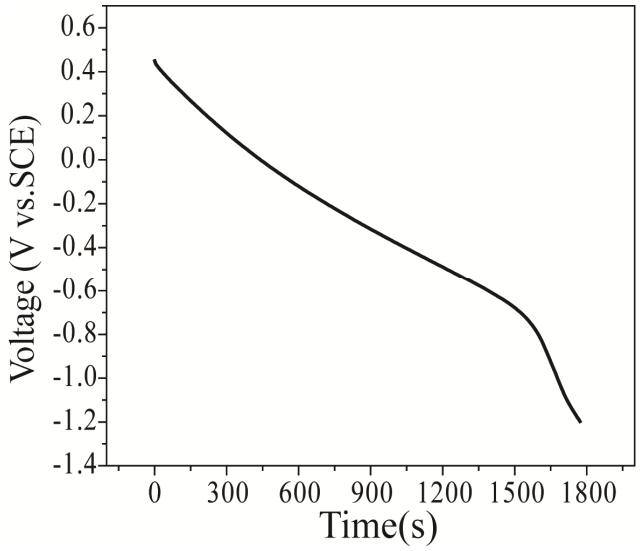

Fig. S5. Galvanostatic discharge profile of ECNT-PPy/5PW_{12} at a current density of 1 mA cm^{-2}.

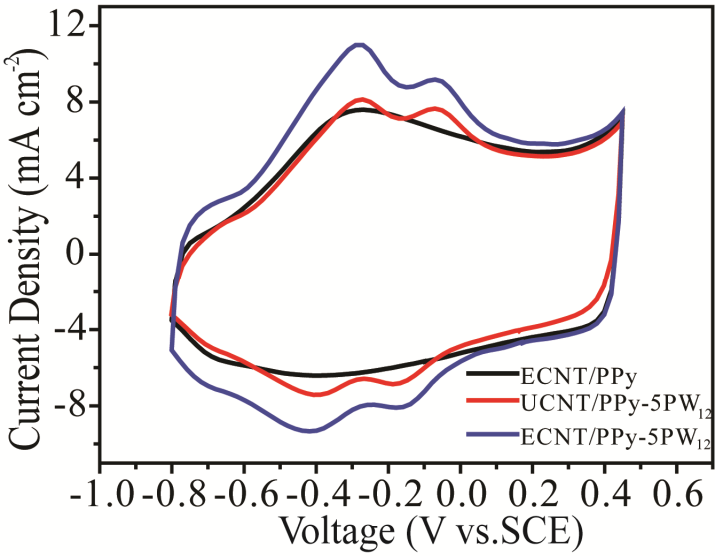

Fig. S6. CV profiles at 5 mV s^{-1} of ECNT-PPy/5PW_{12}, UCNT-PPy/5PW_{12} and ECNT/PPy

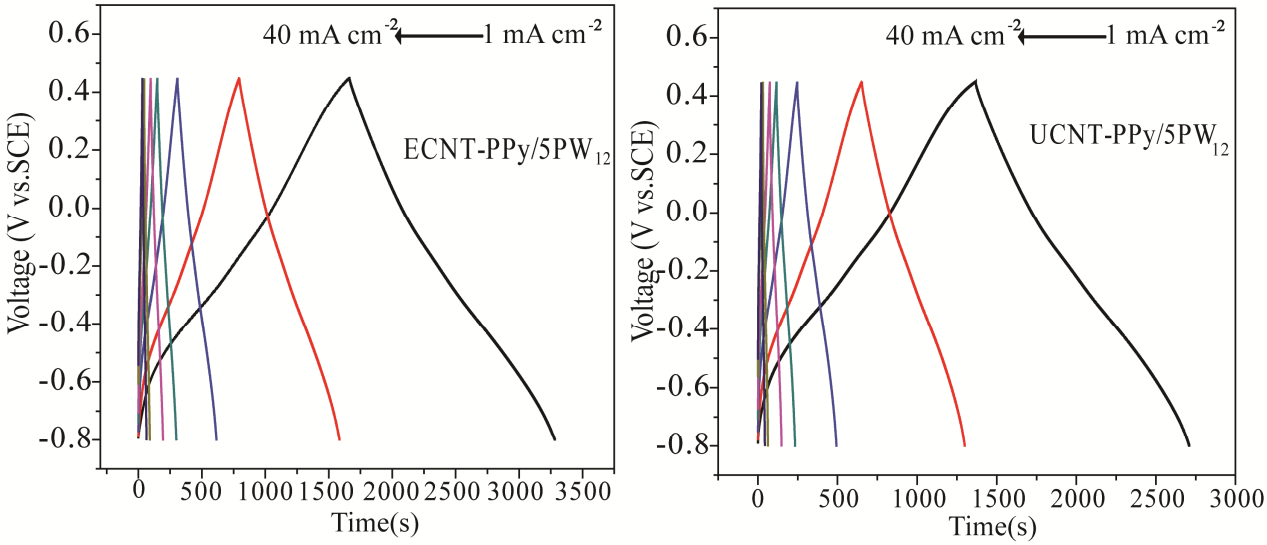

Fig. S7. Galvanostatic charge/discharge curves of ECNT-PPy/5PW_{12} and UCNT-PPy/5PW_{12} at different current densities.

Table. S1. Capacitive performances of recently reported PW_{12} based composite materials and electrochemically fabricated composites of PPy and CNT film

Materials	Capacitance	Rate capability
Cu-MOF/PPy/PW_{12} [1]	1.09 F cm^{-2} (0.5 mA cm^{-2})	68.8% (0.5-2.5 mA cm^{-2})
biochar carbon/PW_{12} [2]	1.19 F cm^{-2} (10 mV s^{-1})	70% (10 -200 mV s^{-1})
PW_{12}/PPy/rGO [3]	295 F g^{-1} (1 A g^{-1})	55% (1-20 A g^{-1})
Polypyrrole nano-pipes/PW_{12} [4]	434 mF cm^{-2} (2 mA cm^{-2})	63% (2-20 mA cm^{-2})
CNT/PPy [5]	637 mF cm^{-2} (1 mA cm^{-2})	75% (1-40 mA cm^{-2})
CNT/PPy [6]	280 mF cm^{-2} (1.4 mA cm^{-2})	43% (1.4 -14 mA cm^{-2})
This work	1300.0 mF cm^{-2} (1 mA cm^{-2})	78.6% (1-40 mA cm^{-2})

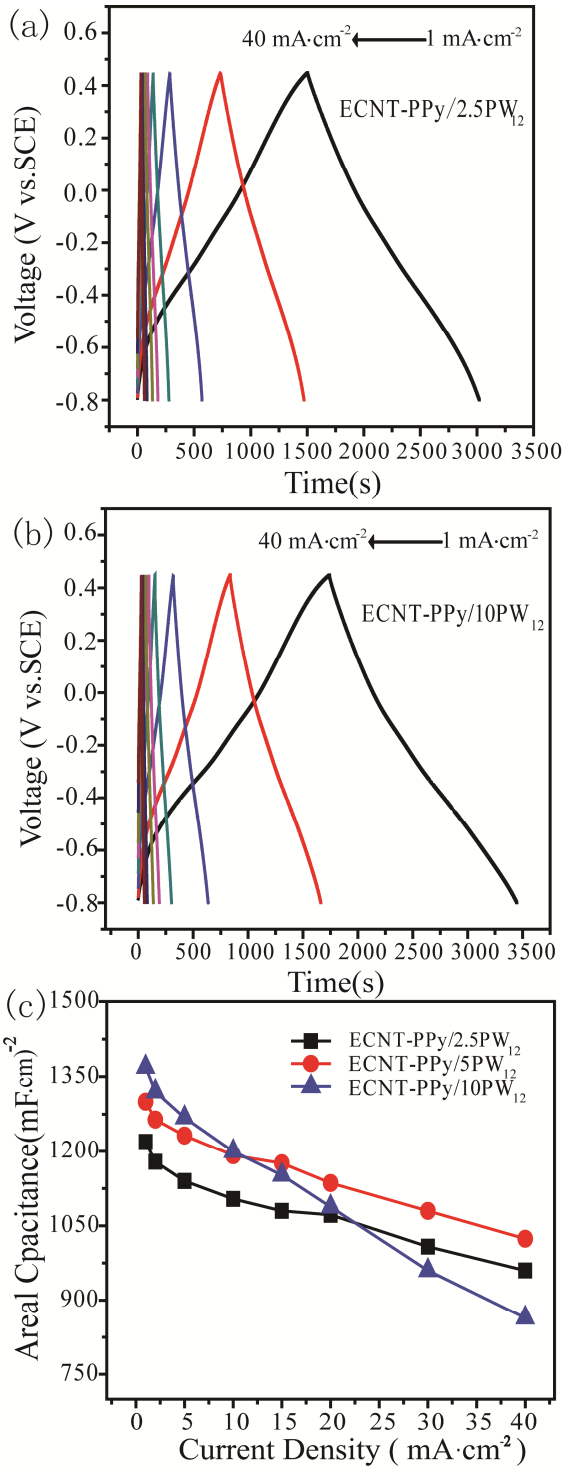

Fig. S8. Galvanostatic charge/discharge curves of ECNT-PPy/2.5PW_{12} (a) and ECNT-PPy/10PW_{12} (b) at different current densities and areal capacitance of ECNT-PPy/2.5PW_{12}, ECNT-PPy/10PW_{12} and ECNT-PPy/10PW_{12} at various current densities ranging from 1 to 40 mA cm^{-2} (c).

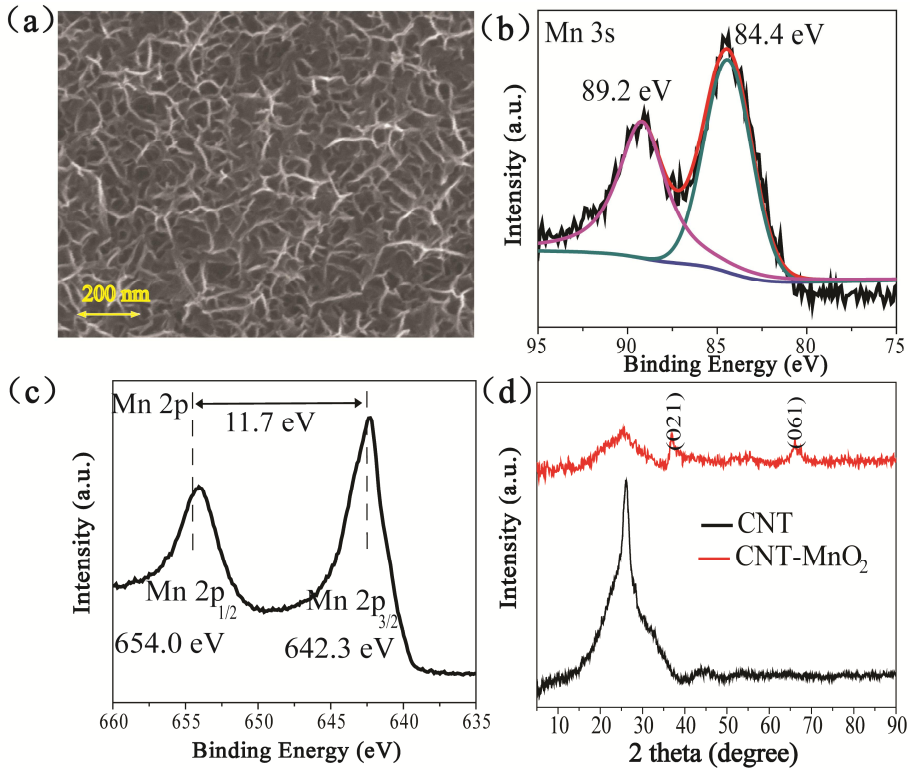

Fig. S9. SEM images of CNT-MnO_2 (a), Mn 3s (b) and Mn 2p (c) XPS core level spectra of CNT-MnO_2 and XRD patterns of CNT and CNT-MnO_2 (d).

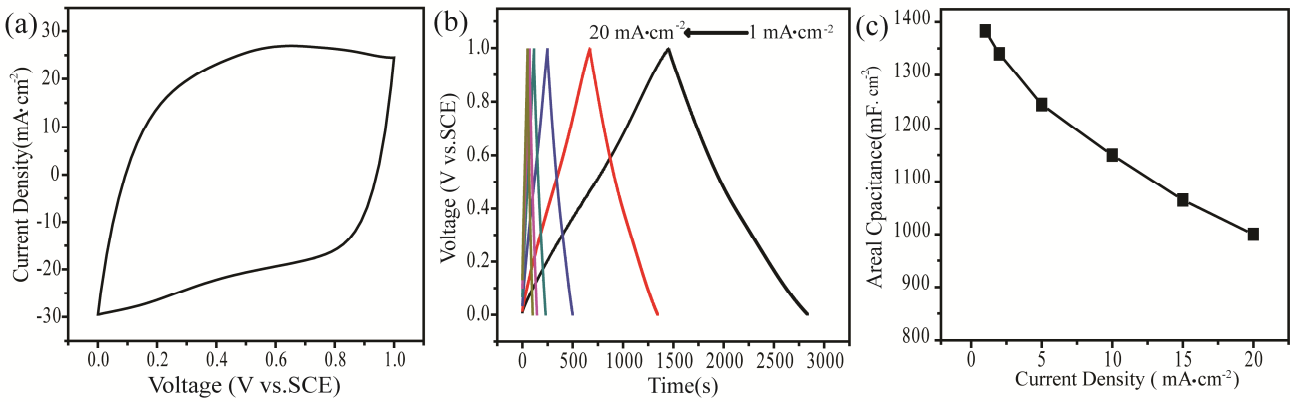

Fig. S10. (a) CV profiles of CNT-MnO_2 at 30 mV s^{-1}; (b) Galvanostatic charge/discharge curves of CNT/MnO_2 at different current density; (c) Areal capacitance of CNT-MnO_2 at various current densities ranging from 1 to 20 mA cm^{-2}.

From SEM images of CNT-MnO_2 shown in Fig. S9a, it could be seen that MnO_2 existed in assembled nanosheets. This could facilitate the penetration of electrode in the active materials for fast faradic reactions. The oxidation state of manganese could be estimated from the spin-energy separation (DE) of Mn 3s signal in XPS spectrum. CNT-MnO_2 displayed a DE of 4.78 eV in its

Mn 3s XPS core level spectrum (Fig. S9b), indicating that the manganese exists in its +4 oxidation state,[7, 8] In the Mn 2p XPS core level spectrum of CNT-MnO_2, Mn $2p_{3/2}$ and Mn $2p_{1/2}$ signals appeared at 642.3 and 654.0 eV, respectively with a DE of 11.7 eV (Fig. S9c). This was in accordance with previously reported MnO_2.[9, 10] The crystal structure of MnO_2 was characterized by XRD. The characteristic diffractions in the XRD pattern (Fig. S9d) could be indexed to (021) and (061) planes of the birnessite-type MnO_2 (JCPDS 14-0644)[11], respectively.

To investigate the electrochemical performances of CNT-MnO_2, electrochemical measures were conducted in a three-electrode system containing 5 M LiCl electrolyte (Fig. S10). Galvanostatic charge/discharge profiles at different current densities are shown in Fig. S10b. The charge profiles were quite symmetric to the discharge ones, demonstrating a good rate capability for CNT-MnO_2. The areal capacitances could be calculated through equ. S1-2, based on the galvanostatic charge/discharge experiments. CNT-MnO_2 displayed an areal capacitance of 1380 mF cm^{-2} at a current density of 1 mA cm^{-2}, and a specific capacitance of 336.58 F g^{-1} at 0.24 A g^{-1}, 60% of its capacitance can be retained when the current density increases 20 times to 20 mA cm^{-2} (Fig. S10c).

References

1. H.-N. Wang, M. Zhang, A. -M. Zhang, F.-C. Shen, X.-K. Wang, S.-N. Sun, Y.-J. Chen and Y.-Q. Lan, *ACS Applied Materials & Interfaces*, 2018, **10**, 32265-32270.
2. M. Genovese and K. Lian, *Journal of Materials Chemistry A*, 2017, **5**, 3939-3947.
3. Y. Chen, M. Han, Y. Tang, J. Bao, S. Li, Y. Lan and Z. Dai, *Chemical Communications*, 2015, **51**, 12377-12380.
4. D. P. Dubal, B. Ballesteros, A. A. Mohite and P. Gómez-Romero, *ChemSusChem*, 2016, **10**, 731-737.
5. Q. Tang, M. Chen, C. Yang, W. Wang, H. Bao and G. Wang, *ACS Applied Materials & Interfaces*, 2015, **7**, 15303-15313.
6. Y. Chen, L. Du, P. Yang, P. Sun, X. Yu and W. Mai, *Journal of Power Sources*, 2015, **287**, 68-74.
7. L. Bao and X. Li, *Advanced Materials*, 2012, **24**, 3246-3252.
8. L. Du, P. Yang, X. Yu, P. Liu, J. Song and W. Mai, *Journal of Materials Chemistry A*, 2014, **2**, 17561-17567.
9. B. Wei, L. Wang, Q. Miao, Y. Yuan, P. Dong, R. Vajtai and W. Fei, *Carbon*, 2015, **85**, 249-260.
10. Z. Lei, J. Zhang and X. -S. Zhao, *Journal of Materials Chemistry*, 2012, **22**, 153-160.
11. S. Chou, F. Cheng and J. Chen, *Journal of Power Sources*, 2006, **162**, 727-734.